ELSEVIER

Journal of Nuclear Materials 313–316 (2003) 685–689

journal of nuclear materials

www.elsevier.com/locate/jnucmat

Influence of plasma pressure gradient on melt layer macroscopic erosion of metal targets in disruption simulation experiments

V.I. Tereshin [a], I.E. Garkusha [a,*], A.N. Bandura [a], O.V. Byrka [a], V.V. Chebotarev [a], V.A. Makhlaj [a], D.G. Solyakov [a], H. Wuerz [b]

[a] *Institute of Plasma Physics of the NSC KIPT, Kharkov 61108, Ukraine*
[b] *Forschungszentrum Karlsruhe, IHM, 76021 Karlsruhe, Germany*

Abstract

Melt layer erosion of metal targets under pulsed high heat loads is discussed. Tungsten, copper, aluminum, and titanium targets were exposed to perpendicular and inclined plasma impact in the quasi-steady-state plasma accelerator QSPA Kh-50. Melt layer motion results in erosion crater formation with rather large mountains of the resolidified material at the crater edge. It is shown that macroscopic motion of the melt layer and surface cracking are the main factors responsible for tungsten erosion.

Keywords: Plasma–materials interaction; Surface effects; Erosion; Divertor

1. Introduction

During such off-normal events as disruptions and vertical displacement events (VDEs) energy flux at the armour material reaches values sufficient for melting of metals and thin melt layer appears at the material surface. The melt layer is subjected to external forces such as surface tension, gradients of both plasma pressure and recoil pressure of evaporating material, Lorentz force and others. Melt motion driven by external forces produces significant macroscopic erosion of materials [1]. This process is considered as the most important one from the point of view of the lifetime of metallic armours [2–5].

Since energy density values expected for ITER-FEAT can not be achieved in existing tokamaks the results obtained with powerful plasma accelerators [6,7] and e-beam facilities [8,9] are used at present for numerical model validation [4] and for experimental simulation of metal targets erosion under high heat loads.

Experimental results on melt layer behavior of metal targets irradiated with a quasi-steady-state plasma accelerator (QSPA) simulating at least in magnitude of heat load, the conditions expected for off-normal events are presented in [10]. It was shown that the surfaces of the resolidified melt layers have a considerable roughness with microcraters and a ridge like relief on the surface. Melt layer erosion by melt motion was clearly identified. However due to the rather small value of the plasma pressure gradient it was masked by boiling, bubble expansion and bubble collapse and by formation of a Kelvin-Helmholtz instability.

In contrast to VDE, during disruptions heating occurs with a characteristic heat load profile having the peak value at the separatrix strike point (SSP). As a consequence, the external pressure and surface tension depend on the position along the melt surface. Results of numerical simulations of disruption have shown that the pressure profiles of the plasma shield after 4 ms are

* Corresponding author. Tel.: +38-0572 356305/726; fax: +38-0572 352664.
E-mail address: garkusha@ipp.kharkov.ua (I.E. Garkusha).

0022-3115/03/$ - see front matter
PII: S0022-3115(02)01361-2

between 4 and 7 bar and the pressure profiles have a half width of 4 cm only [4]. Therefore the plasma pressure gradient should contribute considerably to the macroscopic motion of a melt layer in ITER-FEAT disruptions.

This paper presents experimental results simulating the plasma pressure gradient influence on melt layer erosion and metals behavior under irradiation with high-power plasma streams.

2. Experimental setup

Experiments with tungsten, aluminum, copper, and titanium targets were carried out in the QSPA Kh-50 [6]. Tungsten was chosen since the major part of the ITER-FEAT divertor including the dome, the baffles and the upper parts of the vertical targets are foreseen to be made from this material. Other pure metals with well-known thermo-physial properties were used for determination of common features of melt behavior and for providing additional data for validation of the numerical model.

Main plasma diagnostics used in the present experiments were as follows [6]: the plasma stream velocity was measured by the time-of-flight of the plasma stream between two magnetic probes, the electron density in the plasma stream was evaluated on the basis of Stark broadening of the H_β spectral line, radial distributions of the plasma stream energy density were measured with a movable copper calorimeter, the power density was calculated on the basis of measurements of the time dependencies of the plasma stream density and its velocity. Plasma pressure was measured by piezoelectric detectors.

The parameters of the free hydrogen plasma stream at the target position were as follows: average density of 4×10^{16} cm^{-3}, plasma power density up to 250 GW/m^2, ion energy up to 0.6 keV and duration of the plasma pulse ~0.1–0.14 ms. Plasma stream maximal pressure in near the axis region achieved $(1.6–1.8) \times 10^6$ Pa. The diameter of the QSPA plasma stream was 10–12 cm. The total energy of the plasma stream exceeded 160 kJ. A guiding magnetic field of 0.54 T was applied in these experiments. Shielding layer effects resulting in an essential decrease of energy heat load presented in [6] and well reproduced by numerical simulation are not described here.

Targets were exposed to perpendicular and inclined plasma irradiation with various numbers of pulses. The scheme of the experiment is presented in Fig. 1. Molybdenum protective screens of 12 cm in diameter with central holes of 1, 2 and 3 cm in diameter were used to impose a pressure gradient along the target that mimics the pressure gradient found at the strikepoint locations in a tokamak disruption. The thickness of the molybdenum screen was 2 mm. The distance between the target surface and the molybdenum screen was 3 mm. This distance between the screen and the sample surface was fixed with 4 small insulator bars (not shown in Fig. 1). The diameter of the targets was 5 cm.

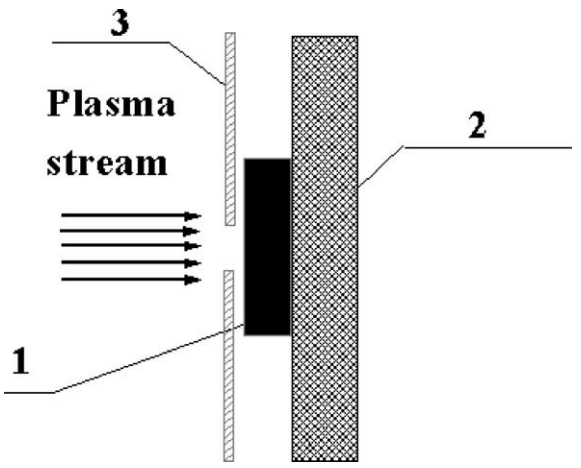

Fig. 1. Scheme of experiment. 1– target, 2 – insulator substrate, 3 – molybdenum screen.

A profilometer with an accuracy of 0.4 μm was used for analysis of the surface of the melt layer. For the sensitive element, a small ball was applied instead of a diamond pin for surface profile measurements to avoid surface roughness contribution to the profilograms. The unexposed part of the target was used as a reference for profilometry. Surface analysis was performed with an optical microscope.

3. Results of experiments

3.1. Perpendicular plasma impact

The image of the tungsten melt spot and the profile of the melt surface are presented in Fig. 2 for perpendicular exposure with 20 pulses. As it follows from profilometry, mountains of melt materials, indicating the melt motion, arise at the melt edge. The distance between mountain peaks is 13 mm (hole diameter is 10 mm). The height of the mountains achieves 50 μm. The high value of the surface roughness ($R_z \sim 30$ μm) masks an erosion crater between the mountains and the ball sensor scans only the roughness peaks. It should be mentioned that even for a target thickness of 7 mm the influence of bending is seen on the profilograms. Sagging of the center of the target is about 10 μm, although initially it has a good flatness. Some drops of splashed tungsten are registered also.

X-ray diffraction analysis of irradiated tungsten has shown a decrease of the tungsten crystal lattice period.

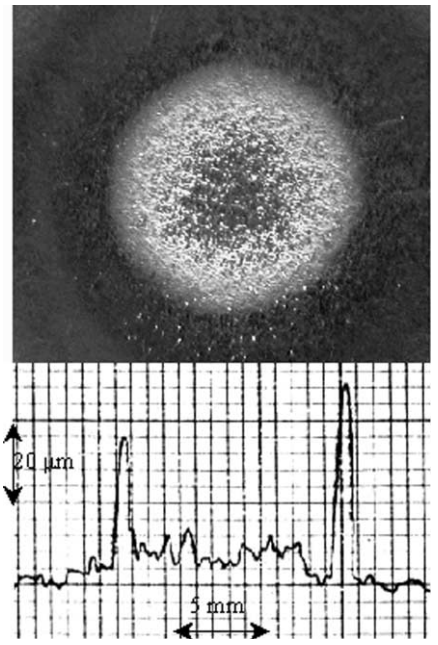

Fig. 2. Image of melt spot and melt layer erosion profile for tungsten target under perpendicular impact of plasma stream. Hole diameter is 1 cm.

This is the result of compressive stresses which arise in the resolidified layer and are accompanied by plastic deformation of material. Appearance of macrostresses leads to crack formation on the tungsten surface. Both fine intergranular and large size cracks are seen on target surfaces (Fig. 3).

Dynamics of the mountains formation dependence on irradiation dose was investigated for irradiation of the Ti sample through a 1 cm hole. The erosion crater with a uniform depth is clearly registered because of the lower level of surface roughness and more pronounced melt motion for titanium. Due to the thermo-mechanical properties of Ti (density, heat conductivity and melt temperature) higher melt velocities and melt layer depth are realized. Erosion crater depth and the distance between mountain peaks increased with the number of pulses and achieved 100 μm and 15 mm respectively after 15 pulses. The height of the mountains achieved 130 μm, their width was of 4–6 mm. With a further increase of the irradiation dose growth of the erosion crater and mountains became slower, because of the resolidified mountain restricts movement of the melt initiated by the next pulse. Both the height of the mountains and their width for Ti essentially exceeded respective tungsten data.

An increase of the hole diameter up to 3 cm results in a non uniform depth of the erosion crater. The profiles are presented in Fig. 4 for exposure with 10 and 20 pulses. The crater with a maximum depth of 150 μm is observed at the periphery of the melt zone close to the mountains. The depth of the erosion crater at the target center is below 50 μm. The height of the mountains (with a width of 6–7 mm) achieved 220 μm. Measurements of plasma pressure distribution along the hole are performed with a piezodetector inserted instead of the target. It shows a steep decrease of pressure value at the 5 mm peripheral zone and a practically constant pressure value in the central region of about 2 cm in diameter. Thus, the most pronounced melt motion is registered in the region of the maximum gradient of plasma pressure.

Similar profiles are obtained also for irradiation of copper and aluminum samples. Mountains due to the melt motion, with a height growing from 40 μm after the first pulse to 250 μm for exposure to 15 pulses are registered for Al target irradiation. Besides, intense boiling with droplet splashing is also observed. High velocities

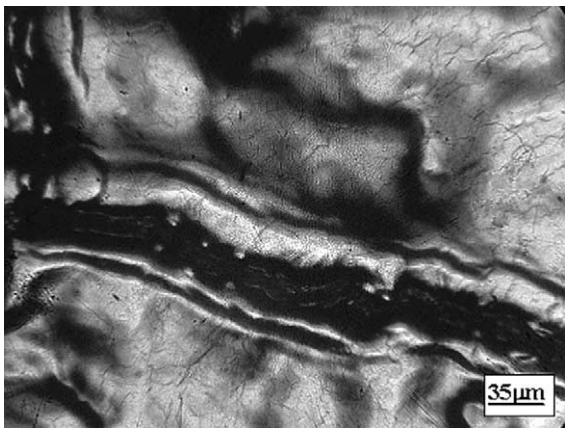

Fig. 3. Image of tungsten melt surface after QSPA irradiation.

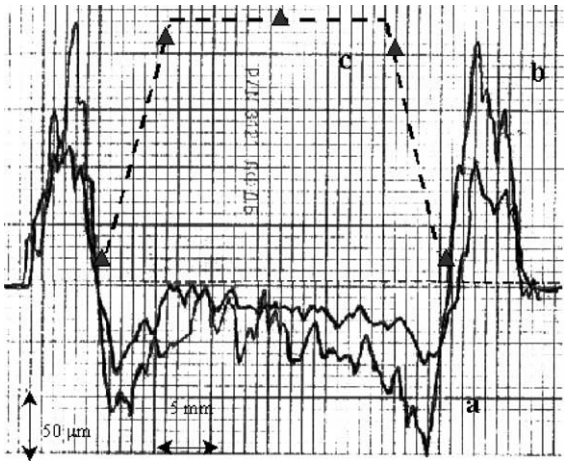

Fig. 4. Melt layer profiles for titanium target irradiated with 10 pulses (curve a) and with 20 pulses (curve b), with overlay of plasma pressure profile (c). Vertical scale for pressure is 3.5 bar/div. Hole diameter is 3 cm.

of Al melt motion and lower melting temperature also add to splashing. Therefore splashing for Al is the most pronounced in comparison with other metals. The droplets size is varied from 5 to 70 μm. The droplet velocity was evaluated on the basis of the droplet size, the distance of their displacement and the duration of the incident plasma stream exposure. The estimated velocity depends on their size and is typically more than 5×10^2 cm/s.

Weight loss measurements of all exposed materials demonstrate inessential contribution of evaporation process to metals erosion.

3.2. Inclined exposure

Melt layer profiles for a tilted Ti target exposed with 10 pulses are shown in Fig. 5. Inclination angle is $\alpha = 20°$ (from parallel to surface incidence). Since the specific heat flux for exposure of an inclined target became essentially less due to both the increase of the plane projection of the plasma stream to the target surface and plasma stream flow around the target, the depth of erosion crater and the height of mountains are also decreased in comparison with perpendicular irradiation with 10 pulses, but less than $\sin\alpha$.

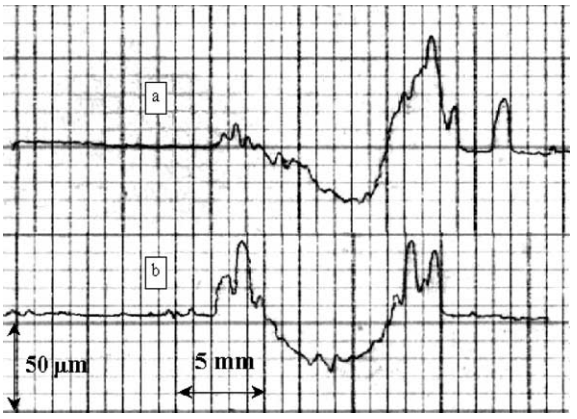

Fig. 5. Melt layer profiles in two mutually perpendicular directions for a Ti target exposed with 10 pulses: (a) direction of inclination, (b) perpendicular direction. Inclination angle $\alpha = 20°$.

Only a 10–15 μm knob is registered at the upstream edge of the melt spot and indicates the contribution of the surface tension to melt motion. Much higher mountain (more than 60 μm) is formed under plasma pressure action at the downstream part of the inclined target. The erosion crater is also asymmetric. Differences in the character of the melt motion for upstream and downstream parts of the inclined Ti target are shown in Fig. 6. The non-melted region is seen at the left side of Fig. 6(a) and at the right side of Fig. 6(b), respectively. A strip-like structure of melt flow showing the motion of the melt stratums driven by the surface tension is observed at the upstream edge. A completely different melt edge picture of the downstream part of the target shows the melt overflow from a mountain peak, producing the streamlets on unexposed parts of the target with droplets at the ends. Such streamlets limit the mountain growth.

4. Conclusions

The experiments have shown that metals erosion is dominated by melt motion. Melt layer motion driven by plasma pressure results in erosion crater formation with rather large mountains of the resolidified material at the crater edge.

Experimental results obtained in e-beam facilities [8] simulating volumetric heating under RAE impact also demonstrate rather pronounced radial motion in the melt layer from the center of melted area to the periphery. But in that case, as indicated in [5], the melt motion occurs mainly due to the surface tension gradient. Under the conditions realized in the QSPA the surface tension gradient is not a determining factor for mountains formation and melt motion is dominated by

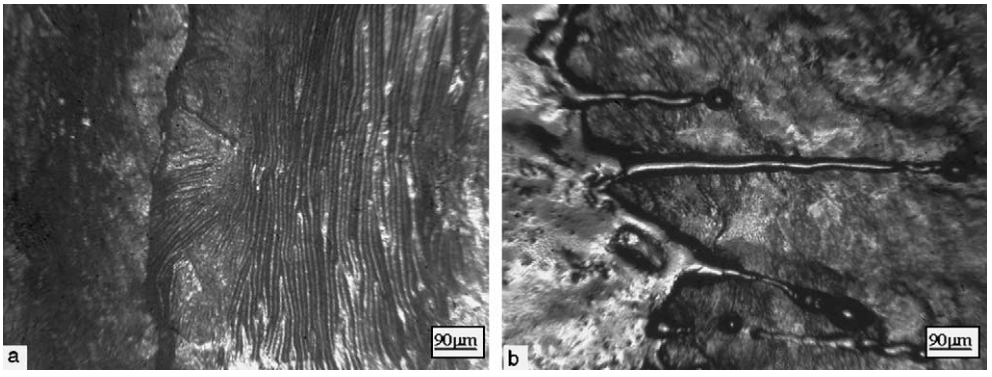

Fig. 6. Edges of melt zone of inclined Ti target after irradiation: (a) upstream part, (b) downstream part.

plasma pressure. For ITER disruptions essentially longer duration of plasma heat load and Lorentz force action should significantly add to the melt motion.

Melt layer motion and surface cracking are the main factors responsible for tungsten damage.

Acknowledgements

This work has been performed within the WTZ projects UKR005-98 and UKR-02-009.

References

[1] H. Wuerz et al., J. Nucl. Mater. 290–293 (2001) 1138.
[2] A.M. Hassanein, Fus. Technol. 15 (1989) 513.
[3] K. Fujimura, M. Ogawa, M. Seki, Fus. Eng. Des. 19 (1992) 183.
[4] H. Wuerz et al., J. Nucl. Mater. 307–311 (2002) 60.
[5] B. Bazylev, H. Wuerz, J. Nucl. Mater. 307–311 (2002) 69.
[6] V.V. Chebotarev et al., J. Nucl. Mater. 233–237 (1996) 736.
[7] N.I. Arkhipov et al., Fus. Eng. Des. 49&50 (2000) 151.
[8] K. Nakamura et al., Fus. Eng. Des. 39&40 (1998) 285.
[9] A. Lodato et al., Fus. Eng. Des. 49&50 (2000) 255.
[10] A.N. Bandura et al., J. Nucl. Mater. 307–311 (2002) 106.